

Oscillation modes of relativistic slender tori

O. M. Blaes^{1*}, P. Arras^{2*} and P. C. Fragile^{3*}

¹*Department of Physics, University of California, Santa Barbara, CA 93106, USA*

²*Kavli Institute for Theoretical Physics, Kohn Hall, University of California, Santa Barbara, CA 93106, USA*

³*Department of Physics and Astronomy, College of Charleston, 58 Coming Street, Charleston, SC 29424, USA*

Accepted —. Received —; in original form —

ABSTRACT

Accretion flows with pressure gradients permit the existence of standing waves which may be responsible for observed quasi-periodic oscillations (QPO’s) in X-ray binaries. We present a comprehensive treatment of the linear modes of a hydrodynamic, non-self-gravitating, polytropic slender torus, with arbitrary specific angular momentum distribution, orbiting in an arbitrary axisymmetric spacetime with reflection symmetry. We discuss the physical nature of the modes, present general analytic expressions and illustrations for those which are low order, and show that they can be excited in numerical simulations of relativistic tori. The mode oscillation spectrum simplifies dramatically for near Keplerian angular momentum distributions, which appear to be generic in global simulations of the magnetorotational instability. We discuss our results in light of observations of high frequency QPO’s, and point out the existence of a new pair of modes which can be in an approximate 3:2 ratio for arbitrary black hole spins and angular momentum distributions, provided the torus is radiation pressure dominated. This mode pair consists of the axisymmetric vertical epicyclic mode and the lowest order axisymmetric breathing mode.

Key words: accretion, accretion discs – black hole physics – relativity – X-rays: binaries.

1 INTRODUCTION

Observations of quasiperiodic oscillations (QPO’s) in the X-ray light curves of black hole and neutron star X-ray binaries have motivated the theory of relativistic “diskoseismology”, the study of hydrodynamic oscillation modes of geometrically thin accretion discs (see Wagoner 1999 and Kato 2001 for reviews). Standing waves with discrete frequencies can exist in such discs because the radial profiles of general relativistic test particle oscillation frequencies can create finite regions where modes are trapped. Because the disc is considered to be geometrically thin, radial pressure gradients are usually negligible in the equilibrium structure of the accretion flow, which is presumed to consist of fluid rotating on nearly circular geodesics.

However, radial pressure gradients themselves can permit the existence of discrete modes because they produce a disc, or torus, of finite extent. At least in the case of black hole X-ray binaries, QPO’s are only observed in the “hard” and “steep power law” spectral/variability states (e.g. McClintock & Remillard 2005), states in which the flow is not solely composed of a standard geometrically thin accretion disc. It is therefore conceivable that radial pressure gradients may be important in trapping modes, and various groups have recently explored the possibility that accretion tori may explain observed QPO’s, e.g. Giannios & Spruit (2004) for low frequency QPO’s, Rezzolla et al. (2003a); Kluźniak et al. (2004); Lee, Abramowicz, & Kluźniak (2004) for high frequency QPO’s. Geometrically thick tori may form in stellar collapse, and modes of dense tori around black holes have also been suggested as a detectable source of gravitational waves (e.g. Zanotti et al. 2003).

A complete analysis of the spectrum of modes in tori has not yet been done except in the limiting case of constant specific angular momentum, slender tori in a Newtonian point mass gravitational potential (Blaes 1985). In this paper we greatly generalize that early work and present a rather complete analysis of the oscillation modes of non-self-gravitating, polytropic,

* E-mail: blaes@physics.ucsb.edu (OMB); arras@kitp.ucsb.edu (PA); fragile@cofc.edu (PCF)

hydrodynamic tori with small cross-section and arbitrary specific angular momentum distributions. The torus equilibria are assumed to be stationary and axisymmetric, and orbit in an arbitrary background spacetime which is itself axisymmetric and possesses reflection symmetry. Although limited to slender tori, our work here could be numerically extended to thicker tori by tracking all the mode frequencies. Armed with a complete understanding of all the mode frequencies and their physical properties, it should be possible to better identify what modes might be responsible for observed QPO's.

An analysis of torus oscillation modes is also useful as a code check for global numerical simulations of accretion flows. In part because of their finite spatial resolution, these simulations generally use tori rather than geometrically thin discs as initial conditions (e.g. De Villiers, Hawley & Krolik 2003; Gammie, McKinney & Tóth 2003). It is noteworthy that global simulations of non-radiative, magnetized accretion flows often produce small, albeit highly variable, hot inner tori near the innermost stable circular orbit (Hawley & Balbus 2002).

This paper is organized as follows. In section 2 we derive the basic equations describing the equilibria and linear perturbations of relativistic slender tori. We then make some general remarks about the types of modes and their classification in section 3. In section 4 we present complete solutions for all the modes of relativistic fluid tori in four special cases where this can be done analytically. Then in section 5 we show how the low order modes of the general torus can be derived exactly, and also present numerical solutions for higher order modes. In section 6 we compare these analytic results with numerical simulations of oscillating hydrodynamic tori, and we finally summarize our conclusions in section 7. Readers who are primarily interested in applications to QPO's should focus on sections 5 and 7. There we identify a robust new candidate for the modes comprising the observed 3:2 ratio of high frequency QPO's in black hole X-ray binaries. We apply our analytic results for these mode frequencies to GRO J1655-40 in Figure 9.

We remind the reader that slender hydrodynamic tori are violently unstable to the Papaloizou-Pringle instability (Papaloizou & Pringle 1984). Perhaps even more important, in the presence of a weak magnetic field, they are unstable to the development of magnetohydrodynamical turbulence due to the magnetorotational instability (Balbus & Hawley 1998). Whether or not the hydrodynamic modes we discuss here can survive these instabilities or even exist is a problem which still needs to be investigated, and we discuss this briefly in section 7.

2 SETTING UP THE PROBLEM

We consider an ideal, hydrodynamic flow in a stationary, axisymmetric spacetime with reflection symmetry. The line element may be expressed as

$$ds^2 = g_{tt}dt^2 + 2g_{t\phi}dtd\phi + g_{rr}dr^2 + g_{\theta\theta}d\theta^2 + g_{\phi\phi}d\phi^2. \quad (1)$$

We take the metric to have signature $(-+++)$. Because of the assumed symmetries, the metric coefficients $g_{\mu\nu}$ depend on r and θ only, and remain unchanged under the transformation $\theta \rightarrow \pi/2 - \theta$.

We will restrict consideration throughout this paper to flows which are isentropic, and in fact polytropic. Hence the internal energy per unit volume e (including rest mass), pressure p , and rest mass density ρ , all measured in the fluid rest frame, are related by

$$e = np + \rho \quad \text{and} \quad p = K\rho^{1+1/n}. \quad (2)$$

Here n is the polytropic index and K is a constant. We use units where $G = c = 1$ here and throughout this paper.

2.1 Equilibrium

We consider an equilibrium, axisymmetric torus in a state of pure rotation. The only nonzero components of the fluid four-velocity are then u^t and u^ϕ . The angular velocity measured by an observer at infinity is $\Omega = u^\phi/u^t$, and the normalization of the four-velocity $u^\alpha u_\alpha = -1$ requires

$$A \equiv u^t = (-g_{tt} - 2\Omega g_{t\phi} - \Omega^2 g_{\phi\phi})^{-1/2}. \quad (3)$$

Other useful quantities are the specific energy \mathcal{E} and specific angular momentum ℓ of a given fluid element:

$$\mathcal{E} \equiv -u_t = (-g^{tt} + 2\ell g^{t\phi} - \ell^2 g^{\phi\phi})^{-1/2} \quad \text{and} \quad \ell \equiv -\frac{u_\phi}{u_t}. \quad (4)$$

The spatial $r - \theta$ structure of the torus is given entirely by the relativistic Euler equation, which in this case may be written

$$\frac{1}{2}\mathcal{E}^2 (\nabla g^{tt} - 2\ell \nabla g^{t\phi} + \ell^2 \nabla g^{\phi\phi}) = -\frac{1}{e+p} \nabla p. \quad (5)$$

Here the operator ∇ may be taken to be either $\partial/\partial r$ or $\partial/\partial \theta$.

In the equatorial plane inside the torus is a special radius r_0 where the pressure has a maximum and fluid orbits on a circular geodesic. From equation (5), the “Keplerian” specific angular momentum ℓ_0 at this radius satisfies

$$(g_{,r}^{tt} - 2\ell_0 g_{,r}^{t\phi} + \ell_0^2 g_{,r}^{\phi\phi})_0 = 0, \quad (6)$$

where subscript zero refers to the pressure maximum.

It is convenient to introduce an effective potential

$$\mathcal{U} = g^{tt} - 2\ell_0 g^{t\phi} + \ell_0^2 g^{\phi\phi}. \quad (7)$$

A test particle with specific angular momentum ℓ_0 orbits on a circular geodesic at an extremum of \mathcal{U} . This extremum is of course located at the pressure maximum r_0 . Linear perturbations of a test particle about this circular geodesic lead to radial and vertical epicyclic oscillations. The squares of the corresponding angular frequencies, as measured by an observer at infinity, are given by

$$\omega_r^2 = \frac{\mathcal{E}_0^2}{A_0^2} \left(\frac{1}{2g_{rr}} \frac{\partial^2 \mathcal{U}}{\partial r^2} \right)_0 \quad \text{and} \quad \omega_\theta^2 = \frac{\mathcal{E}_0^2}{A_0^2} \left(\frac{1}{2g_{\theta\theta}} \frac{\partial^2 \mathcal{U}}{\partial \theta^2} \right)_0, \quad (8)$$

respectively (Abramowicz et al. 2005).

Given our polytropic equation of state (2), the pressure and density can be expressed in terms of an auxiliary function $f(r, \theta)$:

$$p = p_0 f^{n+1} \quad \text{and} \quad \rho = \rho_0 f^n. \quad (9)$$

Consider now a slender torus in which p_0/ρ_0 is very small. By introducing local coordinates measured from the equilibrium point,

$$x \equiv g_{rr0}^{1/2} \left(\frac{r - r_0}{r_0} \right) \quad \text{and} \quad y \equiv g_{\theta\theta0}^{1/2} \left(\frac{\pi/2 - \theta}{r_0} \right), \quad (10)$$

Abramowicz et al. (2005) expanded equation (5) to show that

$$f = 1 - \frac{1}{\beta^2} \left\{ \left[\bar{\omega}_r^2 - \frac{\mathcal{E}_0^2}{A_0^2 \Omega_0^2 \ell_0} \left(\frac{g_{,r}^{tt} - \ell_0 g_{,r}^{t\phi}}{g_{rr}} \frac{\partial \ell}{\partial r} \right)_0 \right] x^2 + \bar{\omega}_\theta^2 y^2 \right\}. \quad (11)$$

Here

$$\beta^2 \equiv \frac{2(n+1)p_0}{\rho_0 A_0^2 r_0^2 \Omega_0^2} \quad (12)$$

is a dimensionless parameter which determines the thickness of the torus. The slender torus limit corresponds to $\beta \rightarrow 0$. The quantities $\bar{\omega}_r$ and $\bar{\omega}_\theta$ are the epicyclic frequencies scaled by the angular velocity at the pressure maximum Ω_0 .

It turns out that the equilibrium function f given by equation (11) can be written more simply and physically. Following Seguin (1975), define the spatial vector

$$\boldsymbol{\gamma} = A\mathcal{E}^3 \left[(1 + \ell\Omega) \boldsymbol{\nabla} g^{t\phi} - \Omega \boldsymbol{\nabla} g^{tt} - \ell \boldsymbol{\nabla} g^{\phi\phi} \right] \quad (13)$$

For barotropic configurations such as the polytropic tori we are considering here, surfaces of constant Ω and ℓ coincide (Abramowicz 1971). By taking the curl of equation (5), it is straightforward to show that the vector $\boldsymbol{\gamma}$ is then perpendicular to these level surfaces,

$$\boldsymbol{\gamma} \times \boldsymbol{\nabla} \ell = 0. \quad (14)$$

Even more importantly, the quantity

$$\kappa^2 \equiv \frac{1}{A^2} \boldsymbol{\gamma} \cdot \boldsymbol{\nabla} \ell = \frac{1}{A^2} \left(\frac{\gamma_r}{g_{rr}} \frac{\partial \ell}{\partial r} + \frac{\gamma_\theta}{g_{\theta\theta}} \frac{\partial \ell}{\partial \theta} \right) \quad (15)$$

represents the characteristic squared frequency (as measured by an observer at infinity) of inertial oscillations in the fluid due to the presence of an equilibrium specific angular momentum gradient. We show this explicitly later in this paper, but the result is not surprising given that $\boldsymbol{\gamma} \cdot \boldsymbol{\nabla} \ell$ is the quantity that appears in relativistic generalizations of the Rayleigh and Høiland local stability criteria (Seguin 1975). At the pressure maximum, equations (6), (13), and (15) imply

$$\kappa_0^2 \equiv \bar{\kappa}_0^2 \Omega_0^2 = \frac{\mathcal{E}_0^2}{\ell_0 A_0^2} \left(\frac{g_{,r}^{tt} - \ell_0 g_{,r}^{t\phi}}{g_{rr}} \frac{\partial \ell}{\partial r} \right)_0. \quad (16)$$

Hence equation (11) may be written as

$$f = 1 - (\bar{\omega}_r^2 - \bar{\kappa}_0^2) \bar{x}^2 - \bar{\omega}_\theta^2 \bar{y}^2, \quad (17)$$

where $\bar{x} \equiv x/\beta$ and $\bar{y} \equiv y/\beta$.

2.2 Perturbations

The equations describing the dynamics of linear perturbations of the torus may be derived by linearizing the relativistic continuity equation,

$$\nabla_\alpha(\rho u^\alpha) = 0, \quad (18)$$

the relativistic Euler equation,

$$u^\beta \nabla_\beta u^\alpha = -\frac{u^\alpha u^\mu + g^{\alpha\mu}}{e+p} \nabla_\mu p \quad (19)$$

the equation of state (2), and the normalization of the four-velocity, about the equilibrium discussed above. Because the equilibrium is stationary and axisymmetric, we choose all the perturbation variables to vary with t and ϕ according to $\exp[i(m\phi - \omega t)]$. Ipser & Lindblom (1992) have shown that the resulting perturbation equations can then be combined into a single, second order partial differential equation in terms of a single scalar perturbation variable. In order to follow the notation of recent work on oscillations of tori (Abramowicz et al. 2005), we define this variable slightly differently as

$$W \equiv -\frac{\delta p}{\rho A \sigma}, \quad (20)$$

where $\sigma \equiv \omega - m\Omega$. We denote this scalar variable by W , as this was the notation first used in the original Newtonian study of global instabilities of tori (Papaloizou & Pringle 1984).

The perturbation equation for tori could be derived by changing variables and taking the appropriate limit of the general equation of Ipser & Lindblom (1992), but we sketch the direct derivation here in order to include some intermediate results which will be useful. The direct derivation is greatly aided by noting that equations (5) and (13) imply

$$-\frac{A\sigma W}{e+p} \nabla p + \nabla(A\sigma W) = A\sigma \nabla W + W\sigma \left[-\frac{\ell}{\mathcal{E}} \gamma + \mathcal{E}(A^2\Omega + g^{t\phi}) \nabla \ell \right] + Wm \left[\frac{1-\ell\Omega}{\mathcal{E}} \gamma + \mathcal{E}(\Omega g^{t\phi} - g^{\phi\phi}) \nabla \ell \right]. \quad (21)$$

Using this and equation (14), it is straightforward to show that the r and θ components of the Eulerian four-velocity perturbation are given by

$$\delta \mathbf{u} = \frac{i\rho}{e+p} \nabla W + \frac{i}{A^2(\sigma^2 - \kappa^2)} \left(\frac{\rho}{e+p} \right) \left\{ \gamma(\nabla \ell \cdot \nabla W) + \sigma A \mathcal{E} W [\sigma(A^2\Omega + g^{t\phi}) + m(\Omega g^{t\phi} - g^{\phi\phi})] \nabla \ell \right\}. \quad (22)$$

The azimuthal component is given by

$$\delta u_\phi = \frac{\rho}{e+p} A \mathcal{E} (\sigma \ell + m\Omega \ell - m) W + \frac{\mathcal{E}^2}{A(\sigma^2 - \kappa^2)} \left(\frac{\rho}{e+p} \right) \nabla \ell \cdot \left\{ A\sigma \nabla W + W \mathcal{E} [\sigma(A^2\Omega + g^{t\phi}) + m(\Omega g^{t\phi} - g^{\phi\phi})] \nabla \ell \right\} \quad (23)$$

These equations are completed by the linearized continuity equation,

$$i \frac{\sigma^2 A^2 \rho^2 n}{(n+1)p} W - i(\sigma \ell + m\Omega \ell - m) \rho (g^{\phi\phi} - g^{t\phi} \Omega) \delta u_\phi + \frac{1}{(-g)^{1/2}} \frac{\partial}{\partial r} [(-g)^{1/2} \rho g^{rr} \delta u_r] + \frac{1}{(-g)^{1/2}} \frac{\partial}{\partial \theta} [(-g)^{1/2} \rho g^{\theta\theta} \delta u_\theta] = 0. \quad (24)$$

So far, these equations are exact. In the slender torus limit, r and θ derivatives of W become dominant in equations (22) and (23), which then imply

$$\delta u_r \sim i \frac{\sigma_0^2}{\sigma_0^2 - \kappa_0^2} \frac{\partial W}{\partial r}, \quad \delta u_\theta \sim i \frac{\partial W}{\partial \theta}, \quad \text{and} \quad \delta u_\phi \sim \frac{\mathcal{E}_0^2 \sigma_0}{\sigma_0^2 - \kappa_0^2} g_0^{rr} \left(\frac{\partial \ell}{\partial r} \right)_0 \frac{\partial W}{\partial r}. \quad (25)$$

Substituting into the linearized continuity equation, transforming coordinates from r and θ to the local, scaled coordinates \bar{x} and \bar{y} , and taking the slender torus limit $\beta \rightarrow 0$, we finally obtain

$$\frac{\bar{\sigma}_0^2}{\bar{\sigma}_0^2 - \bar{\kappa}_0^2} \frac{\partial}{\partial \bar{x}} \left(f^n \frac{\partial W}{\partial \bar{x}} \right) + \frac{\partial}{\partial \bar{y}} \left(f^n \frac{\partial W}{\partial \bar{y}} \right) + 2n \bar{\sigma}_0^2 f^{n-1} W = 0, \quad (26)$$

where $\bar{\sigma}_0 \equiv \sigma_0/\Omega_0 \equiv (\omega - m\Omega_0)/\Omega_0$.

This partial differential equation must be solved together with the boundary condition that the Lagrangian perturbation in pressure at the unperturbed surface vanish:

$$\Delta p|_{f=0} = (\delta p + \xi^\alpha \nabla_\alpha p)|_{f=0} = 0, \quad (27)$$

where ξ^α is the Lagrangian displacement vector. Using the gauge choice $\xi^\alpha u_\alpha = 0$ (Ipser & Lindblom 1992), the r and θ components are given by

$$\boldsymbol{\xi} = \frac{i}{A\sigma} \delta \mathbf{u}. \quad (28)$$

In the slender torus limit, the boundary condition may then be written as

$$\left\{ f^n \left[\frac{\bar{\sigma}_0}{\bar{\sigma}_0^2 - \bar{\kappa}_0^2} \frac{\partial f}{\partial \bar{x}} \frac{\partial W}{\partial \bar{x}} + \frac{1}{\bar{\sigma}_0} \frac{\partial f}{\partial \bar{y}} \frac{\partial W}{\partial \bar{y}} + 2\bar{\sigma}_0 W \right] \right\}_{f=0} = 0. \quad (29)$$

3 GENERAL REMARKS

Equations (17), (26), and (29) describe a global eigenvalue problem for modes of the relativistic, polytropic slender torus. It is important to note that they are, necessarily, *identical* in mathematical form to the corresponding equations for a polytropic slender torus in a Newtonian gravitational potential with axisymmetry and reflection symmetry. All the interesting effects boil down to three characteristic frequencies: the radial epicyclic frequency $\bar{\omega}_r$, the vertical epicyclic frequency $\bar{\omega}_\theta$, and the characteristic frequency of inertial modes at the pressure maximum $\bar{\kappa}_0$.

The slender torus always admits a trivial zero velocity, zero corotating frequency mode, with W being independent of \bar{x} and \bar{y} , and $\bar{\sigma}_0^2 = 0$. In the constant specific angular momentum case, this is the mode which corresponds to the principal mode of the Papaloizou-Pringle instability when the torus has finite thickness (Blaes 1985).

As shown by Abramowicz et al. (2005), the slender torus (even in the baroclinic case) also always admits incompressible modes corresponding to global oscillations of the entire torus at the epicyclic frequencies of the external spacetime:

$$W_r = \bar{x}, \quad \bar{\sigma}_0^2 = \bar{\omega}_r^2 \quad (30)$$

and

$$W_\theta = \bar{y}, \quad \bar{\sigma}_0^2 = \bar{\omega}_\theta^2. \quad (31)$$

The fluid velocity for these modes is spatially constant over a torus cross-section.

Broadly speaking, the remaining modes are of three general types: surface gravity waves, internal inertial waves, and acoustic waves. The last two classes are easily revealed in a WKB analysis of equation (26). Assuming an $\bar{x} - \bar{y}$ dependence proportional to $\exp\{i[\int \bar{k}_x(\bar{x})d\bar{x} + \int \bar{k}_y(\bar{y})d\bar{y}]\}$, and taking the high wavenumber limit $\bar{k} \equiv (\bar{k}_x^2 + \bar{k}_y^2)^{1/2} \rightarrow \infty$, we obtain the local dispersion relation

$$\bar{\sigma}_0^4 - (\bar{k}^2 \bar{c}_s^2 + \bar{\kappa}_0^2) \bar{\sigma}_0^2 + \bar{k}_y^2 \bar{c}_s^2 \bar{\kappa}_0^2 = 0, \quad (32)$$

where

$$\bar{c}_s \equiv \frac{c_s}{\beta A_0 r_0 \Omega_0} = c_s \left(\frac{\rho_0}{2(n+1)p_0} \right)^{1/2} \quad (33)$$

is a scaled local sound speed. This dispersion relation immediately gives two solutions describing the high wavenumber behavior for acoustic and inertial waves:

$$\bar{\sigma}_0^2 = \bar{k}^2 \bar{c}_s^2 \quad \text{and} \quad \bar{\sigma}_0^2 = \frac{\bar{k}_y^2 \bar{\kappa}_0^2}{\bar{k}^2}, \quad (34)$$

respectively. This justifies our claim that $\bar{\kappa}_0$ is the characteristic frequency of inertial oscillations in the fluid.

According to the equilibrium equation (17), surfaces of constant density and pressure have perfectly elliptical cross-section in (\bar{x}, \bar{y}) coordinates. The slender torus equilibrium is therefore perfectly reflection-symmetric about $\bar{x} = 0$ and $\bar{y} = 0$. All the slender torus modes can therefore be assigned a definite parity with respect to each of these reflections, and we note these parities throughout the rest of the paper. In general, thicker tori remain reflection symmetric about the equatorial plane, and so modes will continue to have a definite y -parity. A well-defined x -parity only exists in the slender torus limit, however.

In addition to the parities, we will also label modes with non-negative integer quantum numbers j and k which are derived from the extreme limits of a constant specific angular momentum slender torus in a Newtonian point mass potential and a general slender torus with an incompressible equation of state $n = 0$. These limits are discussed in sections 4.1 and 4.3 below. Physically, $j > 0$ modes have an acoustic character, and have frequencies which diverge in the incompressible limit. Increasing j and k corresponds to shorter spatial scales of variation in the mode eigenfunction on a torus cross-section.

The tori we are analyzing in this paper are violently unstable (Papaloizou & Pringle 1984). This instability is not captured by our equations, because its growth rate happens to vanish in the slender torus limit. However, for tori of finite thickness, the corotation mode becomes the principal mode of the Papaloizou-Pringle instability (Blaes 1985; Goldreich et al. 1986). In addition, the slender torus limit loses the corotation and Lindblad resonances normally associated with nonaxisymmetric spiral waves in discs.

4 COMPLETE SOLUTIONS IN SPECIAL CASES

There are four special cases where a complete solution to the mode spectrum of the slender torus can be derived analytically.

4.1 Constant Specific Angular Momentum in a Newtonian $1/r$ Potential

In a Newtonian $1/r$ potential, the two epicyclic frequencies are both degenerate with the orbital angular velocity: $\bar{\omega}_r = \bar{\omega}_\theta = 1$. If in addition the torus has constant specific angular momentum, then $\bar{\kappa}_0^2 = 0$ and equation (17) implies that isobaric surfaces have circular cross-section in the variables \bar{x} and \bar{y} . By changing variables to (η, θ) given by

$$\bar{x} = \eta \cos \theta \quad \text{and} \quad \bar{y} = \eta \sin \theta, \quad (35)$$

Blaes (1985) showed that the partial differential equation (26) becomes separable and solved the complete eigenvalue problem. The eigenfunctions and eigenfrequencies may be conveniently written as

$$W_{jk} = C_{jk} \eta^k G_j(k+n, k+1, \eta^2) \begin{cases} \cos(k\theta) \\ \text{or} \\ \sin(k\theta) \end{cases} \quad (36)$$

and

$$\bar{\sigma}_0^2 = \frac{1}{n}(2j^2 + 2jn + 2jk + nk) \quad (37)$$

Here C_{jk} is a normalization constant, j and k are non-negative integers, and G_j is a j -th order Jacobi polynomial (Abramowitz & Stegun 1972).

The zero frequency, $j = k = 0$ mode is the corotation mode. The $j = 0, k = 1$ modes correspond to the global radial and vertical epicyclic oscillations of the entire torus, which in this case have frequencies that are degenerate with the orbital angular velocity. Other modes with $j = 0$ have frequencies which are independent of the polytropic equation of state, and represent surface gravity waves. Modes with $k = 0$ and $j \neq 0$ are compressible breathing modes where the torus cross-section expands and contracts. All other modes have a mixed acoustic/surface gravity wave character.

4.2 Keplerian Limit

A specific angular momentum distribution which is at the opposite extreme to that just considered is a ‘‘Keplerian’’ distribution, where every fluid element in the slender torus has the same specific angular momentum as that of a circular geodesic in the equatorial plane. In this case the characteristic frequency of inertial mode oscillations $\bar{\kappa}_0$ is equal to the radial epicyclic frequency $\bar{\omega}_r$. The eigenvalue problem in this limit becomes very simple even in general axisymmetric spacetimes with reflection symmetry.

In the Keplerian limit, the equilibrium function $f = 1 - \bar{\omega}_\theta^2 \bar{y}^2$ only varies with height \bar{y} . One set of modes then has W equal to some linear function of \bar{x} times some function of height \bar{y} . For them, equation (26) becomes

$$\frac{d}{d\bar{y}} \left(f^n \frac{dW}{d\bar{y}} \right) + 2n\bar{\sigma}_0^2 f^{n-1} W = 0. \quad (38)$$

The eigenfunctions are therefore simply Gegenbauer polynomials in \bar{y} (Abramowitz & Stegun 1972),

$$W = C_{n_y}^{(n-1/2)}(\bar{\omega}_\theta \bar{y}) \quad \text{or} \quad \bar{x} C_{n_y}^{(n-1/2)}(\bar{\omega}_\theta \bar{y}), \quad (39)$$

where n_y is a non-negative integer which is equal to the number of vertical nodes. The corresponding eigenfrequencies are

$$\bar{\sigma}_0^2 = \bar{\omega}_\theta^2 \left[\frac{n_y(n_y + 2n - 1)}{2n} \right]. \quad (40)$$

The lowest order, $n_y = 0$ mode is the corotation mode, and $n_y = 1$ gives the vertical epicyclic mode. Higher values of n_y represent standing, vertical acoustic waves. (The eigenfrequencies for the $n_y = 1, 2,$ and 3 vertical oscillations have also been derived by Kato 2005 within Newtonian theory.) The choice of 1 or \bar{x} for the radial dependence indicates that these modes are at least doubly degenerate, and in fact we show numerically in section 5 below that there are many degenerate modes whose frequencies are given by equation (40) at every n_y . In addition, we find that all other modes, apart from the trivial corotation mode, have frequencies which approach the radial epicyclic frequency. Thus the Keplerian limit of the slender torus consists of many degenerate modes at the two epicyclic frequencies and frequencies corresponding to vertical sound waves, plus the corotation mode.

4.3 The Incompressible Torus

In the limit $n \rightarrow 0$, the torus is incompressible and admits only inertial and surface gravity waves (the latter being the $j = 0$ modes discussed in section 4.1 above). These modes can be explicitly calculated for incompressible tori in the general spacetime. In the incompressible limit, equations (26) and (29) become

$$\frac{\bar{\sigma}_0^2}{\bar{\sigma}_0^2 - \bar{\kappa}_0^2} \frac{\partial^2 W}{\partial \bar{x}^2} + \frac{\partial^2 W}{\partial \bar{y}^2} = 0 \quad (41)$$

and

$$\left[\frac{\bar{\sigma}_0}{\bar{\sigma}_0^2 - \bar{\kappa}_0^2} \frac{\partial f}{\partial \bar{x}} \frac{\partial W}{\partial \bar{x}} + \frac{1}{\bar{\sigma}_0} \frac{\partial f}{\partial \bar{y}} \frac{\partial W}{\partial \bar{y}} + 2\bar{\sigma}_0 W \right]_{f=0} = 0. \quad (42)$$

For modes with $\bar{\sigma}_0^2 > \bar{\kappa}_0^2$, it is convenient to change coordinates from \bar{x} to

$$\chi \equiv \left(\frac{\bar{\sigma}_0^2 - \bar{\kappa}_0^2}{\bar{\sigma}_0^2} \right)^{1/2} \bar{x}, \quad (43)$$

so that equation (41) becomes Laplace's equation:

$$\frac{\partial^2 W}{\partial \chi^2} + \frac{\partial^2 W}{\partial \bar{y}^2} = 0. \quad (44)$$

The boundary condition (42) also simplifies:

$$\left[\frac{1}{\bar{\sigma}_0} \frac{\partial f}{\partial \chi} \frac{\partial W}{\partial \chi} + \frac{1}{\bar{\sigma}_0} \frac{\partial f}{\partial \bar{y}} \frac{\partial W}{\partial \bar{y}} + 2\bar{\sigma}_0 W \right]_{f=0} = 0. \quad (45)$$

In terms of χ , the equilibrium function f now becomes, from equation (17),

$$f = 1 - \mathcal{R}^2 \chi^2 - \bar{\omega}_\theta^2 \bar{y}^2, \quad (46)$$

where

$$\mathcal{R} \equiv \left[\frac{\bar{\sigma}_0^2 (\bar{\omega}_r^2 - \bar{\kappa}_0^2)}{\bar{\sigma}_0^2 - \bar{\kappa}_0^2} \right]^{1/2}. \quad (47)$$

It is well-known that Laplace's equation (44) separates in confocal elliptical coordinates (u, v) , defined by

$$\chi = a \cosh u \cos v \quad (48)$$

and

$$\bar{y} = a \sinh u \sin v, \quad (49)$$

where u is a non-negative real number and $0 \leq v < 2\pi$. We choose

$$a = \left(\frac{1}{\mathcal{R}^2} - \frac{1}{\bar{\omega}_\theta^2} \right)^{1/2}, \quad (50)$$

in order that the surface $f = 0$ of the torus corresponds to one of the elliptical coordinate surfaces. This has a fixed value of u given by

$$u = \tanh^{-1} \left(\frac{\mathcal{R}}{\bar{\omega}_\theta} \right) = \frac{1}{2} \ln \left(\frac{\bar{\omega}_\theta + \mathcal{R}}{\bar{\omega}_\theta - \mathcal{R}} \right). \quad (51)$$

The resulting eigenfunctions are then

$$W_k^+ = C_k^+ \cosh(ku) \cos(kv) \quad \text{and} \quad W_k^- = C_k^- \sinh(ku) \sin(kv), \quad (52)$$

where the C 's are again normalization constants and k is again a non-negative integer. The corresponding eigenfrequencies are given by

$$\bar{\sigma}_0^2 = k\mathcal{R}\bar{\omega}_\theta \left[\frac{(\bar{\omega}_\theta + \mathcal{R})^k - (\bar{\omega}_\theta - \mathcal{R})^k}{(\bar{\omega}_\theta + \mathcal{R})^k + (\bar{\omega}_\theta - \mathcal{R})^k} \right]^{\pm 1}. \quad (53)$$

Our derivation of the eigenfunctions (52) and eigenfrequencies (53) assumed that $\bar{\sigma}_0^2 > \bar{\kappa}_0^2$. However, equation (53) generally admits solutions with $\bar{\sigma}_0^2 < \bar{\kappa}_0^2$ as well. The reader may easily repeat the derivation for this case, and verify that the resulting formula for the eigenfrequencies still turns out to be equation (53).

Because \mathcal{R} itself depends on $\bar{\sigma}_0$, equation (53) represents a polynomial equation for the eigenfrequency which must be solved for every k . The universal corotation mode is given by $k = 0$, while $k = 1$ gives the two epicyclic modes. For modes with $k > 1$, $\bar{\sigma}_0^2 > \bar{\kappa}_0^2$ represent surface gravity waves, while $\bar{\sigma}_0^2 < \bar{\kappa}_0^2$ represent internal inertial waves. For reference, we give

Table 1. Lowest Order Modes of the Incompressible Slender Torus.

x -parity	y -parity	k	$\bar{\sigma}_0^2$	Eigenfunction
+	+	0	0	1
-	+	1	$\bar{\omega}_r^2$	\bar{x}
+	-	1	$\bar{\omega}_\theta^2$	\bar{y}
-	-	2	$\{\bar{\omega}_r^2 + \bar{\omega}_\theta^2 \pm [(\bar{\omega}_r^2 + \bar{\omega}_\theta^2)^2 - 4\bar{\kappa}_0^2\bar{\omega}_\theta^2]^{1/2}\}/2$	$\bar{x}\bar{y}$
+	+	2	$\bar{\omega}_\theta^2(4\bar{\omega}_r^2 - 3\bar{\kappa}_0^2)/(\bar{\omega}_\theta^2 + \bar{\omega}_r^2 - \bar{\kappa}_0^2)$	$1 - \frac{(4\bar{\omega}_\theta^2 - \bar{\kappa}_0^2)(\bar{\omega}_r^2 - \bar{\kappa}_0^2)x^2 - \bar{\omega}_\theta^2(4\bar{\omega}_r^2 - 3\bar{\kappa}_0^2)y^2}{2\bar{\omega}_\theta^2 - 2\bar{\omega}_r^2 + \bar{\kappa}_0^2}$

explicit expressions of the eigenfrequencies and eigenfunctions of some of the lowest order incompressible modes for general angular momentum distributions in Table 1.¹

The modes become much simpler in the constant specific angular momentum case $\bar{\kappa}_0 = 0$. Then $\mathcal{R} = \bar{\omega}_r$, and so

$$\bar{\sigma}_0^2 = k\bar{\omega}_r\bar{\omega}_\theta \left[\frac{(\bar{\omega}_\theta + \bar{\omega}_r)^k - (\bar{\omega}_\theta - \bar{\omega}_r)^k}{(\bar{\omega}_\theta + \bar{\omega}_r)^k + (\bar{\omega}_\theta - \bar{\omega}_r)^k} \right]^{\pm 1}. \quad (54)$$

There are no internal inertial modes in this case, and these are all surface gravity waves. In the limit of a Newtonian $1/r$ potential, $\bar{\omega}_r = \bar{\omega}_\theta = 1$, and equation (54) gives the $j = 0$ surface gravity waves of equation (37).

In the Keplerian limit, all the incompressible modes become degenerate with the radial and vertical epicyclic modes. The inertial modes all have frequencies approaching the radial epicyclic frequency, while the surface gravity waves approach either the radial or the vertical epicyclic frequencies.

4.4 Neglecting the Vertical Structure

In an effort to understand the axisymmetric modes seen in numerical studies of tori, Rezzolla et al. (2003b) and Montero et al. (2004) numerically calculated the eigenfunctions and eigenfrequencies of vertically integrated tori. This begs the question - what are the slender torus modes if we ignore the vertical direction?² The problem is easy to solve in general, and is mathematically similar to the Keplerian limit vertical acoustic waves discussed in section 4.2 above. The eigenfunctions are again Gegenbauer polynomials:

$$W = C_{n_x}^{(n_x-1/2)}[(\bar{\omega}_r^2 - \bar{\kappa}_0^2)^{1/2}\bar{x}], \quad (55)$$

where n_x is a non-negative integer equal to the number of radial nodes. The corresponding eigenfrequencies are

$$\bar{\sigma}_0^2 = \bar{\kappa}_0^2 + (\bar{\omega}_r^2 - \bar{\kappa}_0^2) \left[\frac{n_x(n_x + 2n - 1)}{2n} \right]. \quad (56)$$

Note that $n_x = 1$ gives the radial epicyclic mode. Rezzolla et al. (2003b) and Montero et al. (2004) labeled this mode as an f -mode, and higher order modes as o_1, o_2 , etc., i.e. o_{n_x-1} . As they point out, this latter set of modes are physically acoustic (or p -)modes, at least in this two dimensional situation. However, as we show below in the next section, some of these modes are actually related to surface gravity waves in three dimensions, at least in the slender torus limit. This is true in particular of the o_1 mode, which with the radial epicyclic mode they propose might be responsible for the observed 3 : 2 commensurability in high frequency QPO's in black hole X-ray binaries (Rezzolla et al. 2003a).

The ratio in frequencies of the two-dimensional p -modes to the radial epicyclic mode is given by

$$\frac{\bar{\sigma}_0}{\bar{\omega}_r} = \pm \bar{\omega}_r \left[n_x \left(1 + \frac{n_x - 1}{2n} \right) - (n_x - 1) \left(1 + \frac{n_x}{2n} \right) \frac{\bar{\kappa}_0^2}{\bar{\omega}_r^2} \right]^{1/2}. \quad (57)$$

For constant specific angular momentum and $n = 3$, the sequence of frequency ratios is approximately 1.528, 2, 2.449, ..., in good agreement with the (3/2, 4/2, 5/2) sequence that Rezzolla et al. (2003b) claimed was an approximate description of their low order numerical eigenfrequencies. The number 1.528 is also in excellent agreement with the o_1/f ratio found numerically by Montero et al. (2004) (see their Figure 6) to be generic for all slender, vertically integrated, relativistic tori with constant

¹ The reader may be surprised that modes with the same eigenfunction can have different eigenfrequencies, as is the case for the fourth row of Table 1. However, the relationships between W and the Eulerian perturbations δp , eq. (20), and δu_α , eq. (25), depend on frequency, so the fluid perturbations are not the same.

² As Rezzolla et al. (2003b) point out, one must be wary when comparing polytropic, three-dimensional tori with their two-dimensional, vertically integrated representations. In general, the latter do not satisfy a polytropic relationship between vertically integrated pressure and density. In the slender torus limit, however, there is an exact mapping between polytropic equations of state in the equilibrium structure, with $n_{2D} = n_{3D} + 1/2$ (Goldreich et al. 1986). Ignoring the vertical direction is therefore equivalent to adopting the polytropic index n_{2D} . Note that Rezzolla et al. (2003b) and Montero et al. (2004) choose $n_{2D} = 3$ for their numerical results.

Table 2. Eigenfrequencies of the Lowest Order Modes of the General Polytropic Slender Torus.

x -parity	y -parity	j	k	$\bar{\sigma}_0^2$
+	+	0	0	0
-	+	0	1	$\bar{\omega}_r^2$
+	-	0	1	$\bar{\omega}_\theta^2$
-	-	0	2	$\{\bar{\omega}_r^2 + \bar{\omega}_\theta^2 \pm [(\bar{\omega}_r^2 + \bar{\omega}_\theta^2)^2 - 4\bar{\kappa}_0^2 \bar{\omega}_\theta^2]^{1/2}\}/2$
+	+	0	2	$\{(2n+1)(\bar{\omega}_\theta^2 + \bar{\omega}_r^2) - (n+1)\bar{\kappa}_0^2 - [((2n+1)(\bar{\omega}_\theta^2 - \bar{\omega}_r^2) + (n+1)\bar{\kappa}_0^2)^2 + 4\bar{\omega}_\theta^2(\bar{\omega}_r^2 - \bar{\kappa}_0^2)]^{1/2}\}/(2n)$
+	+	1	0	$\{(2n+1)(\bar{\omega}_\theta^2 + \bar{\omega}_r^2) - (n+1)\bar{\kappa}_0^2 + [((2n+1)(\bar{\omega}_\theta^2 - \bar{\omega}_r^2) + (n+1)\bar{\kappa}_0^2)^2 + 4\bar{\omega}_\theta^2(\bar{\omega}_r^2 - \bar{\kappa}_0^2)]^{1/2}\}/(2n)$

specific angular momentum. They also found that the frequency ratio dropped for non-constant specific angular momentum (see their Figure 8), at least for slender tori, consistent with the fact that the frequency ratios in equation (57) all approach unity in the Keplerian limit. We discuss the frequency ratios of the lowest order modes in *three* dimensional tori in the next section.

5 THE LOWEST ORDER MODES OF THE GENERAL PROBLEM

As we noted in section 3, the zero corotation frequency and epicyclic modes are always present for the general torus configuration. One can find additional modes by following the suspicion that a Taylor expansion solution for W about the pressure maximum will generally diverge as the surface $f = 0$ is approached because of the structure of the partial differential equation (26). A solution which is finite there, and therefore able to satisfy the surface boundary condition (29), will therefore probably involve a truncation of the Taylor expansion, i.e. involve only finite polynomials in \bar{x} and \bar{y} . This is in fact true of all the special case modes considered above.

Guided by the fact that the modes must be even or odd, we try an eigenfunction of the form

$$W = a\bar{x}\bar{y}, \quad (58)$$

where a is some constant. This function is odd in both \bar{x} and \bar{y} , and clearly satisfies the boundary condition (29). It gives in fact two modes, with eigenfrequencies determined by the partial differential equation (26):

$$\bar{\sigma}_0^2 = \frac{1}{2} \left\{ \bar{\omega}_r^2 + \bar{\omega}_\theta^2 \pm [(\bar{\omega}_r^2 + \bar{\omega}_\theta^2)^2 - 4\bar{\kappa}_0^2 \bar{\omega}_\theta^2]^{1/2} \right\}. \quad (59)$$

These modes are identical to the odd-odd $k = 2$ modes of the incompressible torus. The positive square root gives a purely incompressible surface gravity wave whose poloidal velocity field from equation (25) is reminiscent of an X-mode polarization gravitational wave. The negative square root gives a purely incompressible inertial mode whose poloidal velocity field represents a circulation around the pressure maximum.

We can go further. Try an eigenfunction of the form

$$W = a + b\bar{x}^2 + c\bar{y}^2, \quad (60)$$

which is even in both \bar{x} and \bar{y} . Here a , b , and c are constants, one of which is arbitrary. Once again, the boundary condition is trivially satisfied. Substituting this function into equation (26), and equating coefficients of 1, \bar{x}^2 and \bar{y}^2 , we end up with three linear homogeneous equations for a , b , and c . Setting the determinant of coefficients to zero, we obtain the eigenfrequencies of the zero corotation frequency mode (for which $b=c=0$), as well as

$$\bar{\sigma}_0^2 = \frac{1}{2n} \left\{ (2n+1)(\bar{\omega}_\theta^2 + \bar{\omega}_r^2) - (n+1)\bar{\kappa}_0^2 \pm \left[\left((2n+1)(\bar{\omega}_\theta^2 - \bar{\omega}_r^2) + (n+1)\bar{\kappa}_0^2 \right)^2 + 4\bar{\omega}_\theta^2(\bar{\omega}_r^2 - \bar{\kappa}_0^2) \right]^{1/2} \right\} \quad (61)$$

The corresponding values of b and c in terms of a are straightforward to calculate, and can be found in Table 3.

The frequency corresponding to the upper sign in equation (61) blows up in the incompressible $n \rightarrow 0$ limit, revealing that it is in general an acoustic mode. It reduces in fact to the acoustic $j = 1$, $k = 0$ mode in the limit of a constant specific angular momentum torus in a Newtonian $1/r$ potential, which we discussed in section 4.1. The velocity field in that case is a breathing mode - the torus cross-section expands and contracts. In the Keplerian limit of section 4.2, the mode frequency becomes that of the $n_y = 2$ vertical acoustic wave.

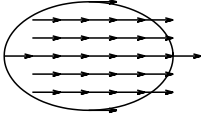
The frequency corresponding to the lower sign in equation (61) reduces to the even-even $k = 2$ mode of Table 1 in the incompressible, $n \rightarrow 0$ limit. This is a gravity wave, and the velocity field in this limit is reminiscent of a +-mode polarization gravitational wave.

We summarize the frequencies and eigenfunctions of all the lowest order modes of the general slender torus in Tables 2 and 3. We also show the poloidal velocity fields for these modes in Figure 1 for a torus with $\bar{\kappa}_0/\bar{\omega}_r = 0.5$. While we are still

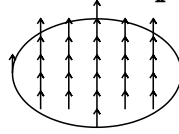
Table 3. Eigenfunctions of the Lowest Order Modes of the General Polytropic Slender Torus.

x -parity	y -parity	(j, k)	Eigenfunction
+	+	(0,0)	1
-	+	(0,1)	\bar{x}
+	-	(0,1)	\bar{y}
-	-	(0,2)	$\bar{x}\bar{y}$
+	+	(0,2) or (1,0)	$1 + \frac{[2n\bar{\sigma}_0^2 - 4(n+1)\bar{\omega}_\theta^2 + \bar{\kappa}_0^2](\bar{\omega}_r^2 - \bar{\kappa}_0^2)\bar{x}^2 - [2n\bar{\sigma}_0^2 - 4(n+1)\bar{\omega}_r^2 + (2n+3)\bar{\kappa}_0^2]\bar{\omega}_\theta^2\bar{y}^2}{2\bar{\omega}_\theta^2 - 2\bar{\omega}_r^2 + \bar{\kappa}_0^2}$

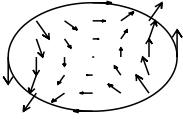
Radial Epicyclic



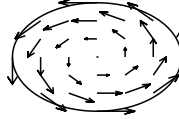
Vertical Epicyclic



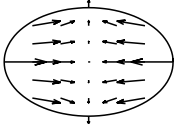
X Mode



Inertial Mode



+ Mode



Breathing Mode

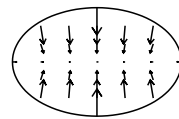


Figure 1. Poloidal velocity fields ($\delta u_x, \delta u_y$) of the lowest order, nontrivial slender torus modes. The torus was assumed to be orbiting in a Kerr spacetime with $a/M = 0.5$ and at a Boyer-Lindquist coordinate radius of $r_0 = 10M$. The slope of the internal specific angular momentum distribution was assumed to give $\bar{\kappa}_0/\bar{\omega}_r = 0.5$ and the polytropic index was $n = 3$.

quite far from the Keplerian limit, the velocity fields are already showing what happens in that case. The X-mode frequency becomes degenerate with $\bar{\omega}_\theta$ in that limit, consisting of opposite vertical oscillations on either radial side of the pressure maximum. The breathing mode becomes degenerate with the lowest order vertical acoustic wave, as its velocity field becomes largely vertical. The inertial and +-modes consist largely of radial motions in the Keplerian limit, and become degenerate with $\bar{\omega}_r$.

It is clear that the procedure we used in this section can be extended to calculate even higher order modes. In the special case of constant specific angular momentum tori, the dispersion relation remains quadratic for modes of quite high order, and we summarize the frequencies and eigenfunctions of these modes in Tables 4 and 5.

In general, however, higher order modes result in dispersion relations which are polynomials of cubic and higher order,

Table 4. Eigenfrequencies of the Lowest Order Modes of the Constant Specific Angular Momentum Slender Torus.

x -parity	y -parity	j	k	$\bar{\sigma}_0^2$
+	+	0	0	0
-	+	0	1	$\bar{\omega}_r^2$
+	-	0	1	$\bar{\omega}_\theta^2$
-	-	0	2	$\bar{\omega}_r^2 + \bar{\omega}_\theta^2$
+	+	0	2	$\{(2n+1)(\bar{\omega}_r^2 + \bar{\omega}_\theta^2) - [4n(n+1)(\bar{\omega}_\theta^2 - \bar{\omega}_r^2)^2 + (\bar{\omega}_r^2 + \bar{\omega}_\theta^2)^2]^{1/2}\}/(2n)$
+	+	1	0	$\{(2n+1)(\bar{\omega}_r^2 + \bar{\omega}_\theta^2) + [4n(n+1)(\bar{\omega}_\theta^2 - \bar{\omega}_r^2)^2 + (\bar{\omega}_r^2 + \bar{\omega}_\theta^2)^2]^{1/2}\}/(2n)$
-	+	0	3	$\{(4n+3)\bar{\omega}_r^2 + (2n+1)\bar{\omega}_\theta^2 - [4n^2(\bar{\omega}_\theta^2 - \bar{\omega}_r^2)^2 + 4n(\bar{\omega}_\theta^2 - \bar{\omega}_r^2)(\bar{\omega}_\theta^2 - 3\bar{\omega}_r^2) + (\bar{\omega}_\theta^2 + 3\bar{\omega}_r^2)^2]^{1/2}\}/(2n)$
-	+	1	1	$\{(4n+3)\bar{\omega}_r^2 + (2n+1)\bar{\omega}_\theta^2 + [4n^2(\bar{\omega}_\theta^2 - \bar{\omega}_r^2)^2 + 4n(\bar{\omega}_\theta^2 - \bar{\omega}_r^2)(\bar{\omega}_\theta^2 - 3\bar{\omega}_r^2) + (\bar{\omega}_\theta^2 + 3\bar{\omega}_r^2)^2]^{1/2}\}/(2n)$
+	-	0	3	$\{(4n+3)\bar{\omega}_\theta^2 + (2n+1)\bar{\omega}_r^2 - [4n^2(\bar{\omega}_\theta^2 - \bar{\omega}_r^2)^2 + 4n(\bar{\omega}_\theta^2 - \bar{\omega}_r^2)(\bar{\omega}_\theta^2 - 3\bar{\omega}_r^2) + (\bar{\omega}_\theta^2 + 3\bar{\omega}_r^2)^2]^{1/2}\}/(2n)$
+	-	1	1	$\{(4n+3)\bar{\omega}_\theta^2 + (2n+1)\bar{\omega}_r^2 + [4n^2(\bar{\omega}_\theta^2 - \bar{\omega}_r^2)^2 + 4n(\bar{\omega}_\theta^2 - \bar{\omega}_r^2)(\bar{\omega}_\theta^2 - 3\bar{\omega}_r^2) + (\bar{\omega}_\theta^2 + 3\bar{\omega}_r^2)^2]^{1/2}\}/(2n)$
-	-	0	4	$\{(4n+3)(\bar{\omega}_\theta^2 + \bar{\omega}_r^2) - [4n(n+3)(\bar{\omega}_\theta^2 - \bar{\omega}_r^2)^2 + 9(\bar{\omega}_\theta^2 + \bar{\omega}_r^2)^2]^{1/2}\}/(2n)$
-	-	1	2	$\{(4n+3)(\bar{\omega}_\theta^2 + \bar{\omega}_r^2) + [4n(n+3)(\bar{\omega}_\theta^2 - \bar{\omega}_r^2)^2 + 9(\bar{\omega}_\theta^2 + \bar{\omega}_r^2)^2]^{1/2}\}/(2n)$

Table 5. Eigenfunctions of the Lowest Order Modes of the Constant Specific Angular Momentum Slender Torus.

x -parity	y -parity	(j, k)	Eigenfunction
+	+	(0,0)	1
-	+	(0,1)	\bar{x}
+	-	(0,1)	\bar{y}
-	-	(0,2)	$\bar{x}\bar{y}$
+	+	(0,2) or (1,0)	$1 + \frac{n\bar{\sigma}_0^2}{\bar{\omega}_\theta^2 - \bar{\omega}_r^2}(\bar{\omega}_r^2 \bar{x}^2 - \bar{\omega}_\theta^2 \bar{y}^2) - \frac{2(n+1)\bar{\omega}_\theta^2 \bar{\omega}_r^2}{\bar{\omega}_\theta^2 - \bar{\omega}_r^2}(\bar{x}^2 - \bar{y}^2)$
-	+	(0,3) or (1,1)	$\bar{x} - \frac{\bar{\omega}_\theta^2[(2n+1)\bar{\sigma}_0^2 - 3(2n+3)\bar{\omega}_r^2]}{\bar{\sigma}_0^2 - 3\bar{\omega}_r^2} \left[\bar{x}\bar{y}^2 + \frac{\bar{\omega}_r^2}{n\bar{\sigma}_0^2 - 3(n+1)\bar{\omega}_r^2} \bar{x}^3 \right]$
+	-	(0,3) or (1,1)	$\bar{y} - \frac{\bar{\omega}_r^2[(2n+1)\bar{\sigma}_0^2 - 3(2n+3)\bar{\omega}_\theta^2]}{\bar{\sigma}_0^2 - 3\bar{\omega}_\theta^2} \left[\bar{x}^2 \bar{y} + \frac{\bar{\omega}_\theta^2}{n\bar{\sigma}_0^2 - 3(n+1)\bar{\omega}_\theta^2} \bar{y}^3 \right]$
-	-	(0,4) or (1,2)	$\bar{x}\bar{y} - \frac{(2n+3)\bar{\omega}_\theta^2(\bar{\sigma}_0^2 - \bar{\omega}_r^2) - 3(2n+5)\bar{\omega}_r^2 \bar{\omega}_\theta^2}{3(\bar{\sigma}_0^2 - \bar{\omega}_r^2 - 3\bar{\omega}_\theta^2)} \bar{x}^3 \bar{y} - \frac{(2n+3)\bar{\omega}_\theta^2(\bar{\sigma}_0^2 - \bar{\omega}_\theta^2) - 3(2n+5)\bar{\omega}_r^2 \bar{\omega}_\theta^2}{3(\bar{\sigma}_0^2 - \bar{\omega}_\theta^2 - 3\bar{\omega}_r^2)} \bar{x} \bar{y}^3$

and should be solved numerically. To do this, we substitute the power-series expansion

$$W(\bar{x}, \bar{y}) = \sum_{i,l=0}^{\infty} W_{il} \bar{x}^i \bar{y}^l. \quad (62)$$

in equation (26), and equate coefficients of $\bar{x}^i \bar{y}^l$. We find the following set of algebraic equations

$$\begin{aligned} & \frac{\bar{\sigma}_0^2}{\bar{\sigma}_0^2 - \bar{\kappa}_0^2} [(i+1)(i+2)W_{i+2,l} - (\bar{\omega}_r^2 - \bar{\kappa}_0^2)i(i-1)W_{il} \\ & - \bar{\omega}_\theta^2(i+1)(i+2)W_{i+2,l-2}] + (l+1)(l+2)W_{i,l+2} \\ & - (\bar{\omega}_r^2 - \bar{\kappa}_0^2)(l+1)(l+2)W_{i-2,l+2} - \bar{\omega}_\theta^2 l(l-1)W_{il} \\ & - 2n \frac{\bar{\sigma}_0^2}{\bar{\sigma}_0^2 - \bar{\kappa}_0^2} (\bar{\omega}_r^2 - \bar{\kappa}_0^2) i W_{il} - 2n \bar{\omega}_\theta^2 l W_{il} + 2n \bar{\sigma}_0^2 W_{il} = 0, \end{aligned} \quad (63)$$

which can be written as a matrix equation $A(\bar{\sigma}_0)W = 0$, defining the matrix A . We solve equation (63) with basis vectors for $i = i_1 + 2(I-1)$ and $l = l_1 + 2(L-1)$, where $I = 1, \dots, I_{\max}$, $L = 1, \dots, L_{\max}$. Here $i_1 = 0$ for even x -parity and 1 for odd x -parity, and similarly for l_1 . Our numerical technique to solve equation (63) is to sweep through frequency space and look for zeros of the determinant of the matrix $A(\bar{\sigma}_0)$.

Figure 2 shows eigenfrequencies found by solving equation (63) compared to the various analytical results. The solutions are greatly simplified in the Keplerian limit, as many different branches converge together. The lowest clump approaches the radial epicyclic mode at ω_r . Inertial modes approach ω_r from below in the Keplerian limit and go to zero in the constant specific angular momentum limit. Surface gravity waves approach ω_r from above in the Keplerian limit. The next grouping is around the vertical epicyclic mode at ω_θ . Surface gravity waves approach this frequency from above. The next two groupings shown are sound waves with 2 and 3 vertical nodes. The frequency increases as more horizontal nodes are added, giving the ‘‘fan’’ away from the Keplerian limit. The lowest order sound wave is nearly independent of κ_0 , and higher order modes are more sensitive.

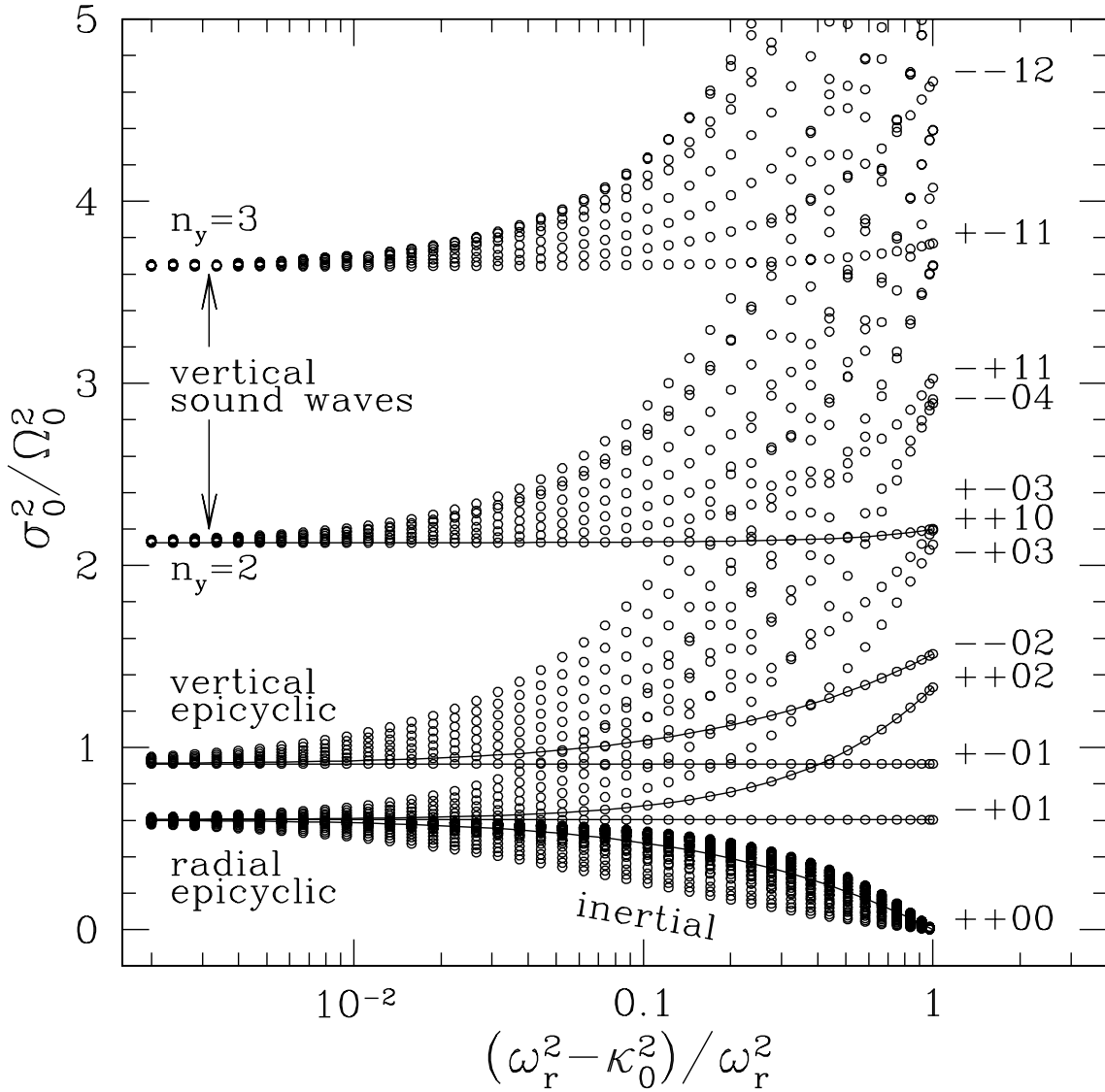


Figure 2. Slender torus eigenfrequencies as a function of $(\omega_r^2 - \kappa_0^2)/\omega_r^2$, which ranges from the Keplerian limit (left) to the constant specific angular momentum limit (right). Circles show the numerical solution to equation (26), assuming four basis functions for \bar{x} and \bar{y} . Lines show the exact analytic solutions in Table 2. Vertical sound waves in the Keplerian limit are labeled by the number of vertical nodes $n_y = 2, 3$ (see equation 40). Labels on the right hand side are for modes in a constant specific angular momentum torus (Table 4). The black hole was taken to have $a/M = 0.9$ and the torus centre was at $r = 10M$, giving $\bar{\omega}_r^2 = 0.604$ and $\bar{\omega}_\theta^2 = 0.910$. The polytropic index was $n = 3$. The corotation mode ($\bar{\sigma}_0^2 = 0$) is not shown, but is also present for all specific angular momentum distributions.

5.1 Mode Frequency Ratios

Based on the behavior of its counterpart in vertically integrated tori, Rezzolla et al. (2003a) and Zanotti et al. (2005) identify the “plus-mode” surface gravity wave as a p -mode, which they label as the o_1 mode. For compressible tori, this characterization is not entirely inaccurate. While the radial compressions present in this mode are always accompanied by vertical expansions in three dimensions, these vertical expansions can be much smaller than the radial motions if the torus is very compressible, as shown in Figure 1.

It is this mode and the radial epicyclic mode that Rezzolla et al. (2003a) propose might be responsible for the 3:2 frequency ratio observed in high frequency QPO’s of black hole X-ray binaries. Figure 3 depicts this frequency ratio computed from equation (61) for slender, constant specific angular momentum tori of different polytropic indices, orbiting Kerr black holes with various spin parameters, as a function of the radius of the torus. As Rezzolla et al. (2003a) found numerically in various specific cases, the frequency ratio is indeed close to 1.5. Relativity is essential here, as the ratio drops to $2^{1/2}$ in the

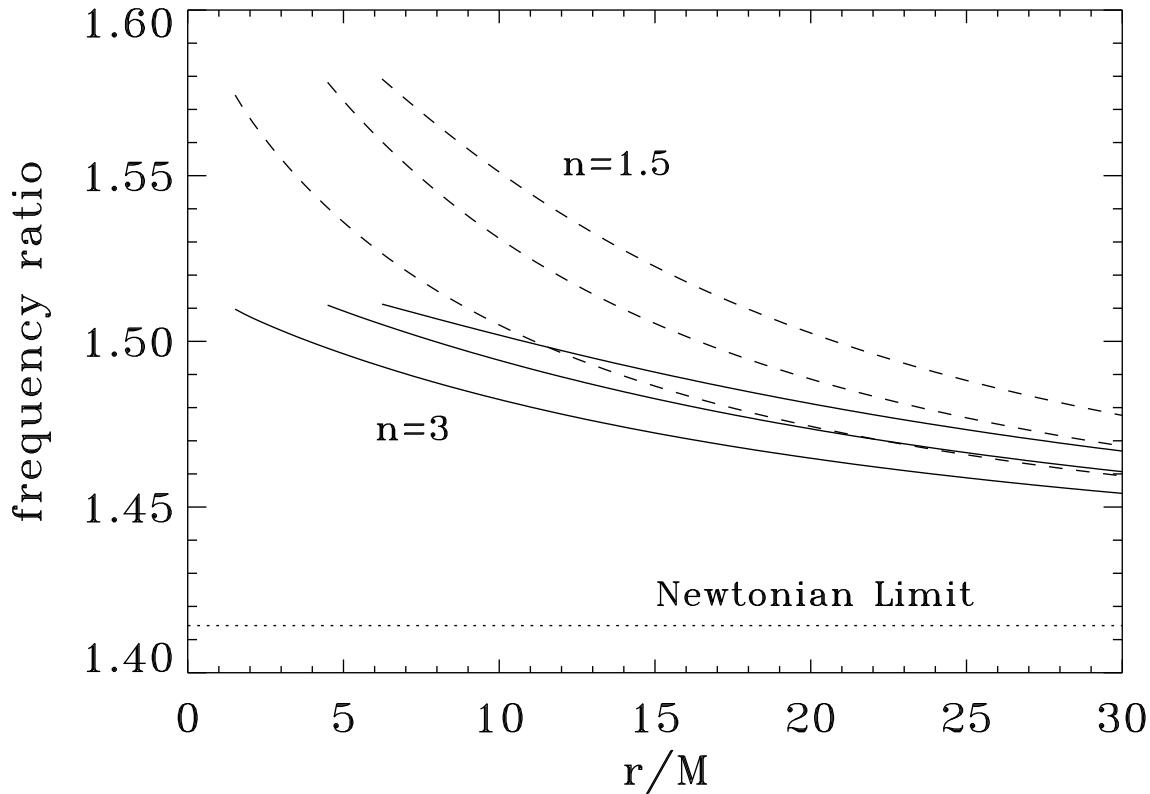


Figure 3. Ratio of the “plus mode” surface gravity wave ($+, +, j = 0, k = 2$) frequency to the radial epicyclic mode frequency, for a slender constant specific angular momentum ($\kappa_0^2 = 0$) torus in a Kerr spacetime at different Boyer-Lindquist coordinate radii. Solid curves are for a polytropic index $n = 3$, while dashed curves are for $n = 1.5$. From top to bottom, each of the three curves at fixed n corresponds to spin parameters $a/M = 0, 0.5$, and 0.998 , respectively. The Newtonian limit of the frequency ratio, $2^{1/2}$, is indicated by the horizontal dotted line.

Newtonian limit of large torus radii (see eq. 37 with $j = 0$ and $k = 2$). As shown in Figure 4, the frequency ratio also drops for non-constant specific angular momentum, approaching unity in the Keplerian limit $\bar{\kappa}_0^2 = \bar{\omega}_r^2$.

Our general mode analysis reveals that there is another pair of modes whose frequency ratio is not too far from 1.5: the “breathing mode” acoustic wave and the vertical epicyclic mode. Figures 5 and 6 show the ratios of these two mode frequencies for a variety of equilibrium parameters. For $n = 3$ tori in particular, which are probably most relevant to radiation pressure supported configurations, the frequency ratio is close to 1.5 even in the Keplerian limit. This is in contrast to the plus-mode/radial epicyclic mode pair, whose ratio goes to unity in the Keplerian limit. (The reader should compare Figures 4 and 6, and note the different scalings on the vertical axis.)

These are but just two examples of possible mode pairs which may be related to the observed 3 : 2 commensurability of high frequency QPO’s in black hole X-ray binaries. There are presumably others. In particular, we have only considered axisymmetric ($m = 0$) frequency ratios in this section, but of course $m \neq 0$ would allow an even richer set of possibilities.

6 COMPARISON WITH NUMERICAL SIMULATION

A number of authors have performed axisymmetric numerical simulations of hydrodynamic tori in order to explore their oscillation modes. Different techniques have been used to excite the oscillations. For example, Zanotti et al. (2005) tried initial radial velocity perturbations, initial density perturbations, and perturbations based on the eigenfunctions of the modes of vertically integrated tori. Lee, Abramowicz, & Kluźniak (2004) and Rubio-Herrera & Lee (2005a,b) have also tried periodic external forcing of the inner regions of the torus at a specific frequency.

Here we use the analytic solutions from section 5 to excite a spectrum of modes in slender hydrodynamic tori and then allow them to evolve numerically for a large number of orbital periods. The goals are to verify that we can indeed identify the modes at subsequent stages of simulation and lay the foundation for further numerical study of more general

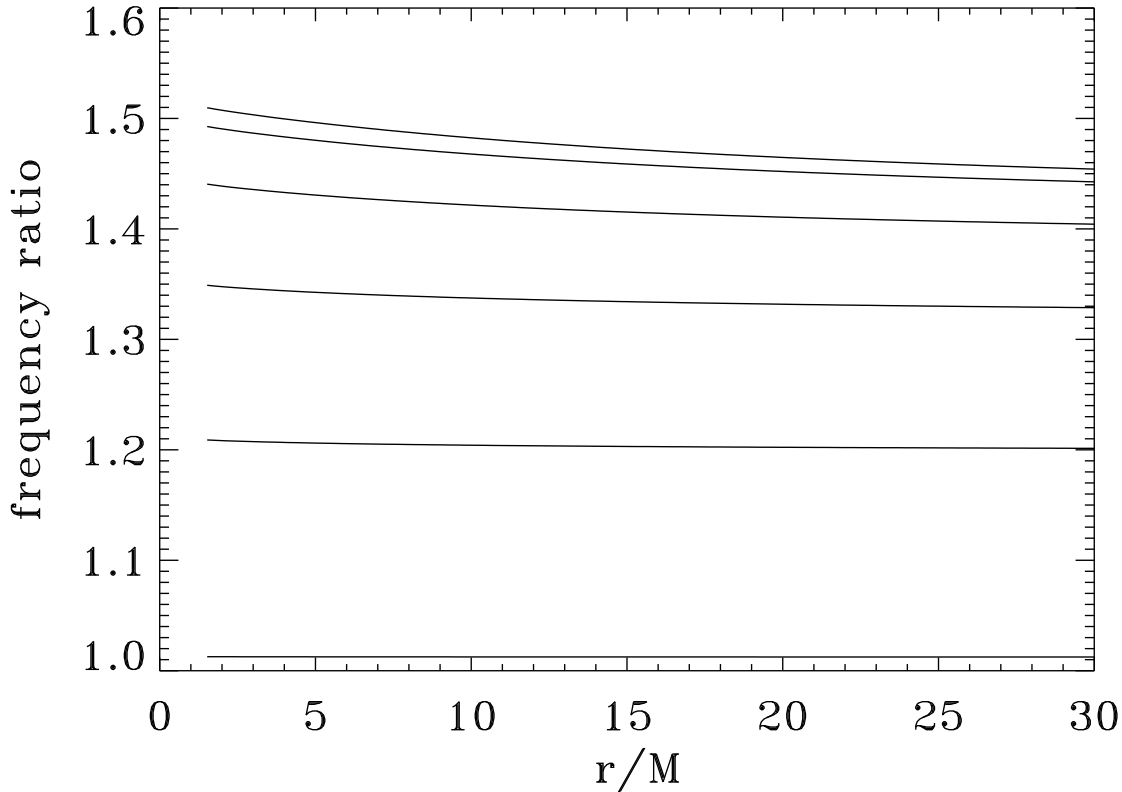


Figure 4. Ratio of the “plus mode” surface gravity wave (+, +, $j = 0, k = 2$) frequency to the radial epicyclic mode frequency, for a slender $n = 3$ torus in an $a/M = 0.998$ Kerr spacetime at different Boyer-Lindquist coordinate radii and different values of κ_0 . From top to bottom, the curves have $\kappa_0/\omega_r = 0, 0.2, 0.4, 0.6, 0.8,$ and 0.99 .

torus configurations. The numerical evolution was carried out using the *Cosmos++* relativistic magnetohydrodynamic code described in Anninos, Fragile, & Salmonson (2005).

The present simulations are restricted to two-dimensional axisymmetry in order to expedite this work and avoid the growth of non-axisymmetric instabilities (Papaloizou & Pringle 1984). We use a single-level fixed mesh with a resolution of 128^2 . We use a Schwarzschild spacetime, and the Schwarzschild coordinate grid covers an angular scale $0.488\pi \leq \theta \leq 0.512\pi$ and has radial boundaries at $r_{min} = 9.7M$ and $r_{max} = 10.3M$. The pressure maximum of the unperturbed torus is located at $r_0 = 10.0M$, while its inner radius is $r_{in} = 9.9M$. The orbital period at the pressure maximum is $\tau_{orb} = 199M$. The polytropic index is $n = 3$ and the polytropic constant is chosen such that the sound speed at the pressure maximum is $c_{s,0} = 0.0011$. The specific angular momentum distribution is chosen to be a power law,

$$\ell = \ell_0 \left(\frac{\lambda}{\lambda_0} \right)^{2-q},$$

where, for Schwarzschild spacetime, $\lambda \equiv (-g^{tt}/g^{\phi\phi})^{1/2}$.

We initially excite a set of modes by using the eigenfunctions of Tables 3 or 5. The phase of the oscillation modes are initially chosen such that the perturbations only need to be applied to the velocity fields and not density or pressure. Following Zanotti et al. (2005), we tracked the modes by looking at the Fourier transform of the norm of the rest-mass density $\|\rho\|^2 \equiv \sum_{i=1}^{N_r} \sum_{j=1}^{N_\theta} \rho_{ij}^2$ and making a comparison with the predicted mode frequencies. As we show, this method successfully identifies many of the desired modes, but does a poor job on others. It also reveals power spectrum peaks that do not correspond to the initial set of modes that were excited.

Figure 7 shows a portion of the power spectrum of $\|\rho\|^2$ for a simulation of a non-constant specific angular momentum torus ($l_0 = 3.95$ and $q = 1.929$, so that $\bar{\kappa}_0/\bar{\omega}_r = 0.5$). Each of the eigenfrequencies from Table 2 is labeled. Figure 8 shows a similar power spectrum for a constant specific angular momentum torus ($l = 3.95$) with each of the eigenfrequencies from Table 4 indicated. While many of the eigenfrequencies are clearly present in the power spectrum, several are not. In particular, the vertical epicyclic mode (01+-) is not obvious, even though it was definitely excited by the initial conditions. We suspect that this is due to the fact that this mode produces very little in terms of density changes, and so the $\|\rho\|^2$ diagnostic is not sensitive to its presence. (The fact that the radial epicyclic mode is still easily detected is probably due to the squeezing of the

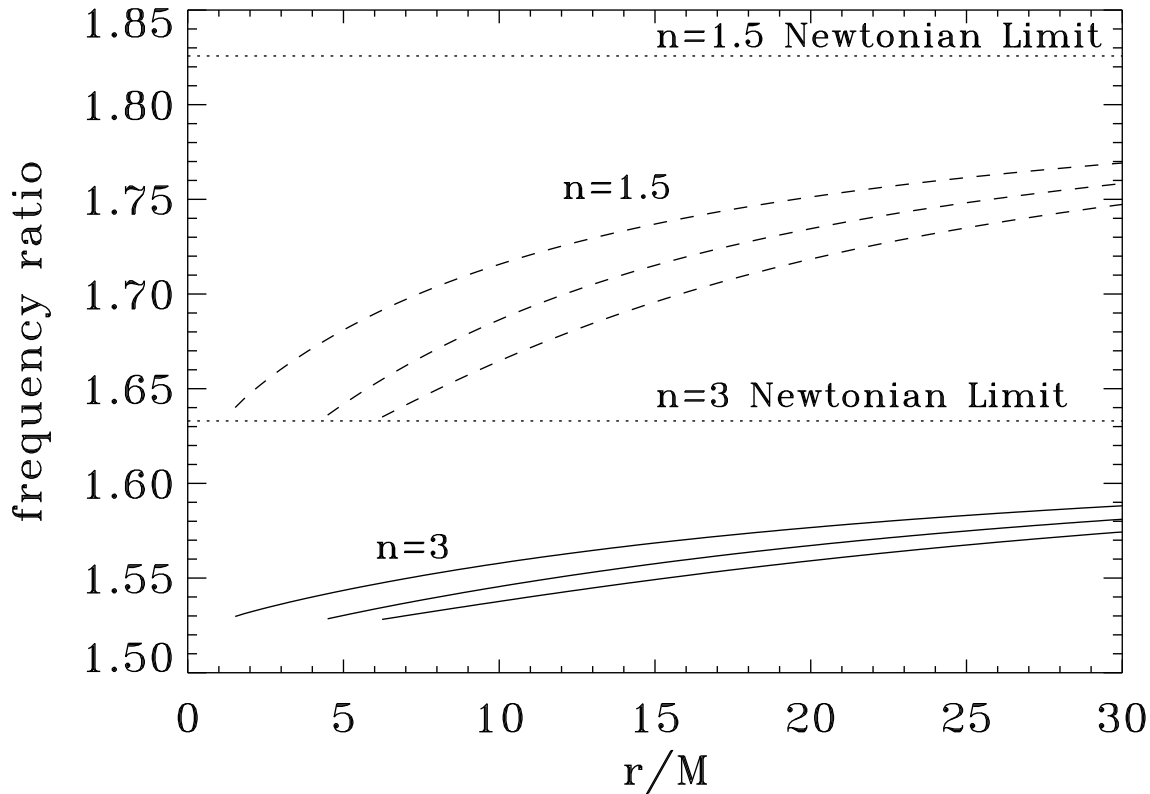


Figure 5. Ratio of the “breathing mode” acoustic wave (+, +, $j = 1, k = 0$) frequency to the vertical epicyclic mode frequency, for a slender constant specific angular momentum ($\kappa_0^2 = 0$) torus in a Kerr spacetime at different Boyer-Lindquist coordinate radii. Solid curves are for a polytropic index $n = 3$, while dashed curves are for $n = 1.5$. From top to bottom, each of the three curves at fixed n corresponds to spin parameters $a/M = 0, 0.5$, and 0.998 , respectively. The Newtonian limits of the frequency ratios from equation (37), $(8/3)^{1/2}$ for $n = 3$ and $(10/3)^{1/2}$ for $n = 1.5$, are shown by the horizontal dotted lines.

torus by the increasing tidal field of the black hole during the inward phase of the oscillation.) We also tried using $\|\rho - \rho_i\|^2$ as a diagnostic, where ρ_i is the initial density field of the torus, and found that the vertical epicyclic mode was much stronger in the resulting power spectrum, while other modes were missing. More work needs to be done to investigate more sensitive numerical diagnostics for these modes.

The prominent peaks at $f/f_0 \simeq 0.53, 1.40$ and 1.80 in Figure 7 are likely not true oscillation modes. The nonlinear interaction of two waves with frequencies f_1 and f_2 , if not forbidden by selection rules (parity, etc.), will produce modulation at “combination frequencies” $|f_1 \pm f_2|$. The three peaks may then be explained as $f_{10++} - f_{01+-} = 1.53 - 1.00 \simeq 0.53$, $0.53 + f_{02++} = 0.53 + 0.88 \simeq 1.41$, and $2f_{02++} = 2 \times 0.88 \simeq 1.76$, respectively. Alternatively, we find numerically that there is a higher order even-even parity mode with frequency 1.78 , implying a near resonance with $2f_{02++}$. Lastly, we note that there is a chance near resonance $f_{01-+} + f_{02++} \simeq f_{10++}$. In the slender torus, this interaction is forbidden by the parity selection rule for the radial direction. However, this parity rule is strictly valid only for the infinitely slender torus, and may still occur in our numerical simulations.

7 DISCUSSION AND CONCLUSIONS

We have presented a rather complete discussion of the oscillation modes of non-self-gravitating, relativistic, polytropic tori in an arbitrary axisymmetric spacetime with reflection symmetry, in the limit where the tori are very slender. Non-slender torus oscillation modes can be explored numerically, and some work on this has already been done by Zanotti et al. (2005) and Rubio-Herrera & Lee (2005b). It would also be possible to examine the behavior of modes for thicker tori analytically using perturbative methods, generalizing the technique employed by Blaes (1985).

All the slender tori considered in this paper are hydrodynamically unstable to the nonaxisymmetric, Papaloizou-Pringle instability (PPI) (Papaloizou & Pringle 1984). They would also develop magnetohydrodynamical turbulence in the presence of a weak magnetic field because of the MRI (Balbus & Hawley 1998). Almost all simulations examining oscillations of tori,

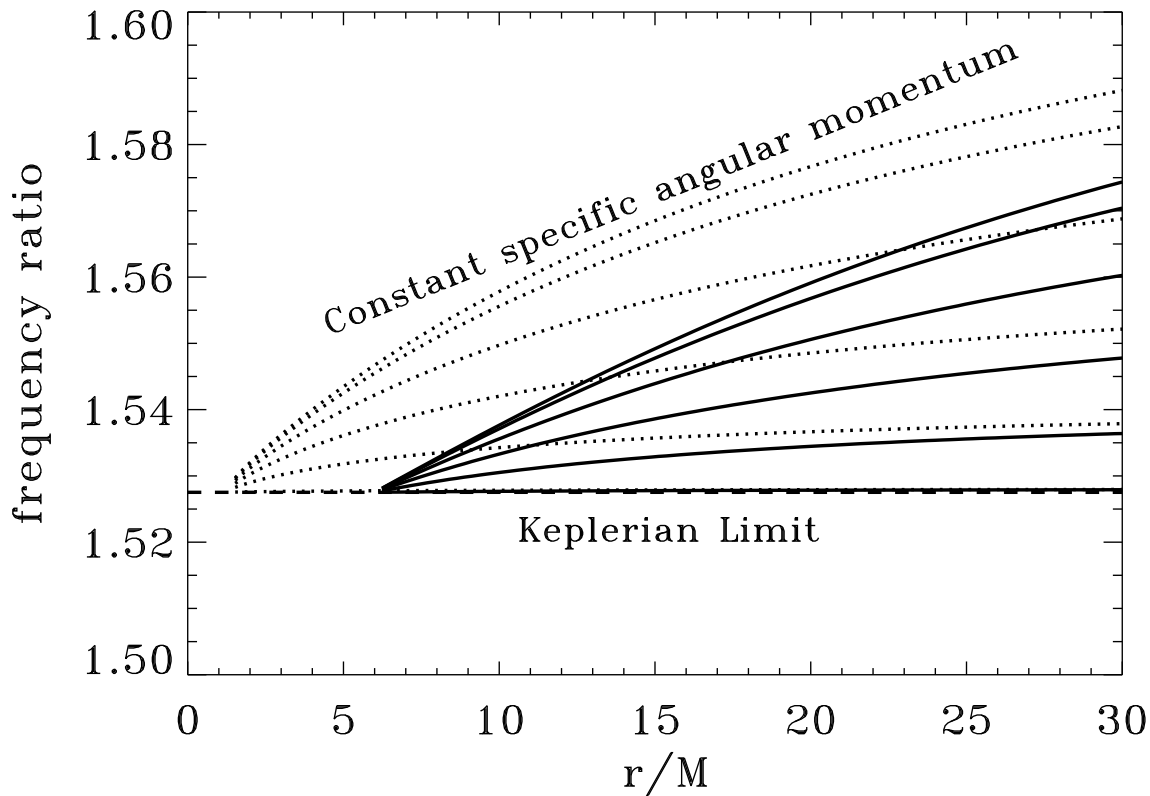


Figure 6. Ratio of the “breathing mode” acoustic wave (+, +, $j = 0, k = 2$) frequency to the vertical epicyclic mode frequency, for a slender $n = 3$ torus in an $a/M = 0.998$ Kerr spacetime (dotted curves) and a Schwarzschild spacetime (solid curves) at different Boyer-Lindquist coordinate radii and different values of κ_0 . From top to bottom, the curves have $\kappa_0/\omega_r = 0, 0.2, 0.4, 0.6, 0.8,$ and 0.99 . The $\kappa_0/\omega_r = 0.99$ curves are of course close to the Keplerian limit (eq. 40 with $n_y = 2$), shown as the horizontal dashed line.

including those presented in this paper, have been axisymmetric and neglected magnetic fields, so both of these instabilities have not been allowed to develop. A major outstanding issue is therefore which, if any, of the hydrodynamic torus modes survive these instabilities. A preliminary investigation of this has been done by Fragile (2005), but more work needs to be done. At least in radially extended tori, the PPI can be suppressed by dynamical accretion through the torus inner edge (Blaes 1987; De Villiers & Hawley 2002). Moreover, the MRI appears to dominate the PPI when magnetic fields are included, and generally leads to a near-Keplerian distribution of specific angular momentum in the flow (Hawley & Balbus 2002). If modes which are essentially hydrodynamic in nature can exist in the presence of MRI turbulence, then the near Keplerian limit is therefore probably of most interest. The turbulence itself may then determine the mode amplitudes, but all of these questions remain to be investigated. A systematic understanding of all the types of modes which may be present, as we have done in this paper, should aid such investigations.

Figure 2 shows that all mode families converge to the epicyclic frequencies or vertical sound waves in the Keplerian limit. If physical discs are indeed nearly Keplerian, this greatly simplifies seismology as only a few distinct frequencies exist. But how close are real discs to the Keplerian limit? Equation (8) can be rewritten in terms of the angular momentum gradient for Keplerian motion, $\partial l_K / \partial r$, by differentiating equation (6) and substituting into equation (8). The result is exactly the same as for κ in equation (16), with $\partial l / \partial r$, the angular momentum gradient for the fluid torus, replaced by $\partial l_K / \partial r$. The difference of these two quantities becomes

$$\omega_r^2 - \kappa_0^2 = \frac{E_0^2}{l_0 A_0^2} \left(\frac{g_{,r}^{tt} - l g_{,r}^{t\phi}}{g_{rr}} \right)_0 \frac{\partial}{\partial r} (l_K - l), \quad (64)$$

which manifestly goes to zero in the Keplerian limit.

De Villiers, Hawley & Krolik (2003) present plots of l_K and l (averaged against density over spherical shells) against radius for MRI driven accretion onto Kerr black holes. In the region of the “inner torus” (see their Figure 3), they find l has a similar slope as l_K , but is smaller by $\sim 1 - 10\%$, the difference going to zero at the marginally stable orbit. Using equation 64, this implies $(\omega_r^2 - \kappa_0^2) / \omega_r^2 \sim 0.01 - 0.1$ in our notation. Hence Figure 2 shows that low order modes should be quite accurately

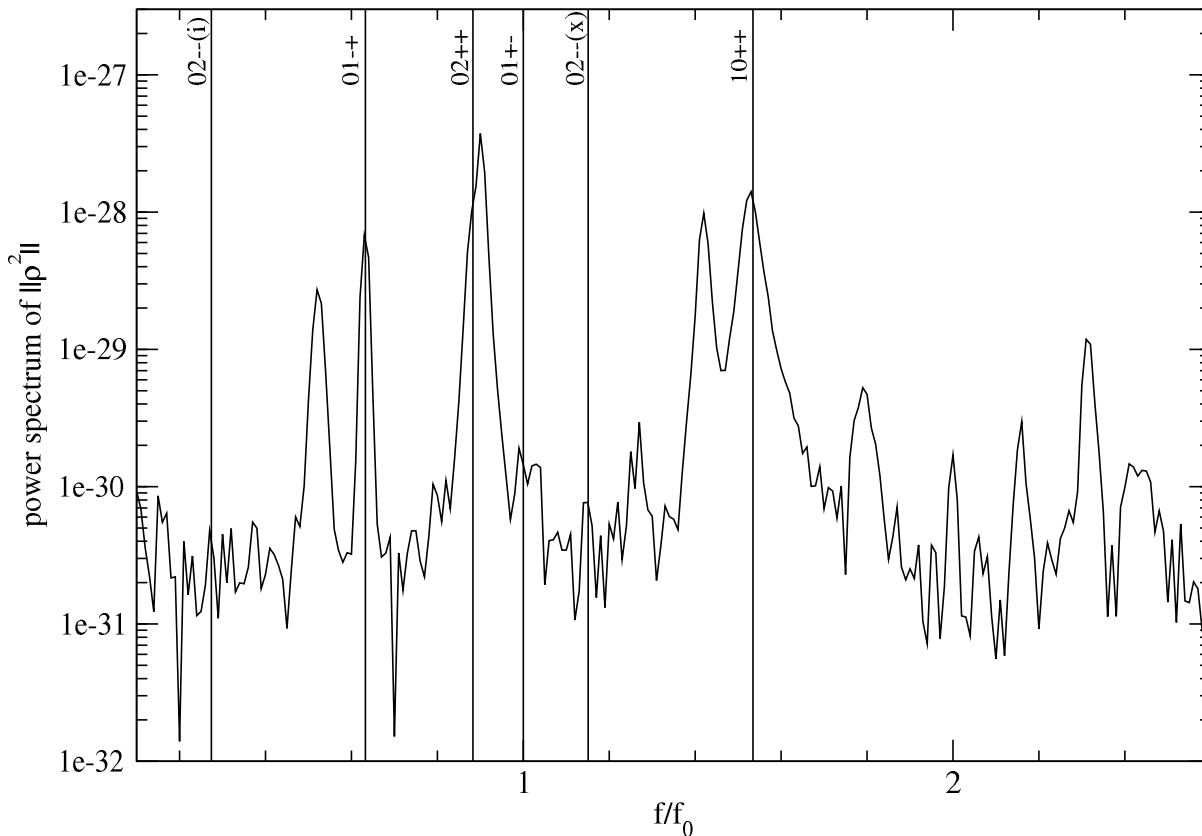


Figure 7. Power spectrum of $||\rho||^2$ for a torus with $\kappa_0/\bar{\omega}_r = 0.5$. Each of the eigenfrequencies from Table 2 are identified. The units of the vertical axis are arbitrary, while the horizontal axis has been scaled with the reciprocal of the orbital period at the pressure maximum.

described by the Keplerian limit, while the deviation from the Keplerian limit increases with number of nodes. For emission from an optically thick region, flux variations from the photosphere become smaller as more angular nodes are included due to averaging of hot and cold spots. Hence low order modes, which are more nearly in the Keplerian limit, are also likely more observable.

In view of this, the lowest order breathing mode/vertical acoustic wave and the vertical epicyclic mode may be an attractive candidate for a pair of modes which have a near 3:2 commensurability for radiation pressure-dominated ($n = 3$) tori, as this persists in the Keplerian limit. This is in contrast to the plus mode and radial epicyclic mode pair, whose frequency ratio approaches unity in the Keplerian limit. Identifying the vertical epicyclic mode with the lower of the two observed frequencies also allows the black holes to have any spin parameter, in contrast to the case where the lower of the two frequencies is identified as the radial epicyclic mode. This is illustrated in Figure 9 for the case of GRO J1655-40. This source has a mass of $\sim 6.3 M_\odot$ (Orosz 2003), and models which identify the 300 Hz QPO as the axisymmetric radial epicyclic mode require $a/M \gtrsim 0.9$ (Rezzolla et al. 2003a; Török 2005). The same is true for diskoseismology models which identify the 300 Hz QPO with an axisymmetric “ g -mode”, which has a frequency below the radial epicyclic frequency within the mode trapping region (e.g. Wagoner, Silbergleit & Ortega-Rodríguez 2001). This is in conflict with recent continuum spectral fitting results which suggest a lower black hole spin (Shafee et al. 2005). If the 300 Hz QPO is instead the axisymmetric vertical epicyclic mode, any spin is possible. Many other mode pairs would probably also work, especially if we consider nonaxisymmetric ($m \neq 0$) modes. However, one still needs to explain why the QPO’s occur at the actual observed frequencies, i.e. what singles out a preferred radius for the torus in this source.

More work needs to be done to investigate how torus oscillation modes might manifest themselves in X-ray light curves and power spectra. Some work has been done based on tracking photon geodesics from the torus to the observer (Bursa et al. 2004; Schnittman & Rezzolla 2005), but additional work needs to be done on the photon emission mechanism of the tori themselves. The difficulties that some diagnostics have in identifying torus oscillation modes in numerical simulations, even when they are present in the initial conditions as discussed in section 6 above, should serve as a warning to numericists searching for QPO’s in their simulations. The X-ray observations generally have nothing to do with these diagnostics.

It remains unclear whether tori are appropriate models for the flow geometry for the “steep power law state” (McClintock & Remillard 2005) where high frequency QPO’s are seen in black hole X-ray binaries. Kubota & Done (2004) suggest that the steep power

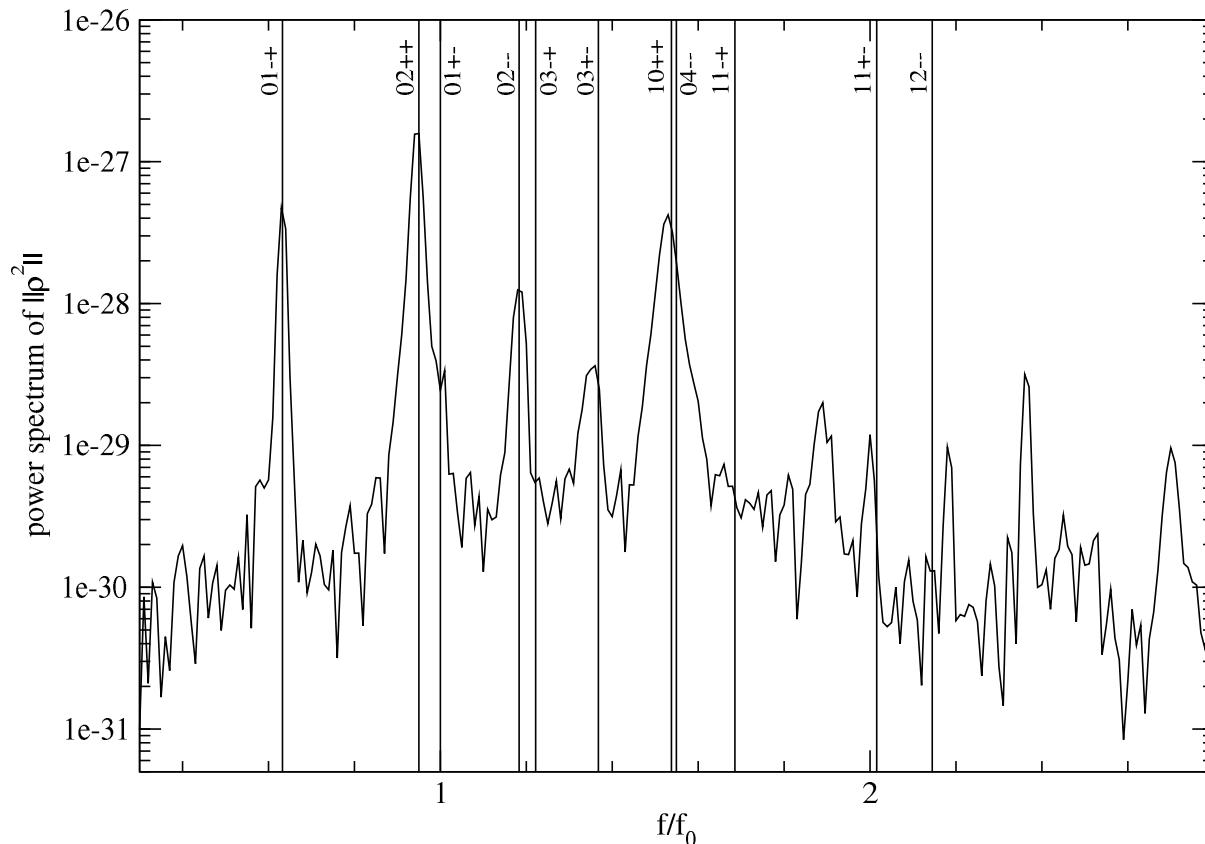


Figure 8. Similar to Figure 7, but for a constant specific angular momentum torus with each of the eigenfrequencies from Table 4 identified.

law state consists of a standard geometrically thin disc sandwiched between a magnetized corona which has sucked up much of the accretion power out of the disc. Oscillation modes that are analogous to the torus modes with vertical reflection symmetry *might* exist in such a magnetized corona, because the vertical velocities vanish in the equatorial plane, where the high inertia disc is located. We hope that our comprehensive hydrodynamic mode analysis may act as a foundation for investigation of these and the other questions noted above.

ACKNOWLEDGMENTS

We thank Marek Abramowicz, Włodek Kluźniak, Luciano Rezzolla, Shin Yoshida, and Olindo Zanotti for very useful discussions. This research was supported in part by the National Science Foundation under grants PHY99-0794 and AST03-07657, and under the following NSF programs: Partnerships for Advanced Computational Infrastructure, Distributed Terascale Facility (DTF) and Terascale Extensions: Enhancements to the Extensible Terascale Facility.

REFERENCES

- Abramowicz, M. A., 1971, *Acta Astronomica*, 21, 81
- Abramowicz, M. A., Blaes, O. M., Horák, J., Kluźniak, W., & Rebusco, P., 2005, *Classical and Quantum Gravity*, submitted
- Abramowicz, M., & Stegun, I. A., 1972, *Handbook of Mathematical Functions* National Bureau of Standards, Washington, DC
- Aninos, P., Fragile, P. C., & Salmonson, J. D., 2005, *ApJ*, 635, 723
- Balbus, S. A., & Hawley, J. F., 1998, *Rev. Mod. Phys.*, 70, 1
- Blaes, O., 1985, *MNRAS*, 216, 553
- Blaes, O. M., 1987, *MNRAS*, 227, 975
- Bursa, M., Abramowicz, M. A., Karas, V., & Kluźniak, W., 2004, *ApJ*, 617, L45
- De Villiers, J.-P., & Hawley, J. F., 2002, *ApJ*, 577, 866
- De Villiers, J.-P., Hawley, J. F., & Krolik, J. H., 2003, *ApJ*, 599, 1238

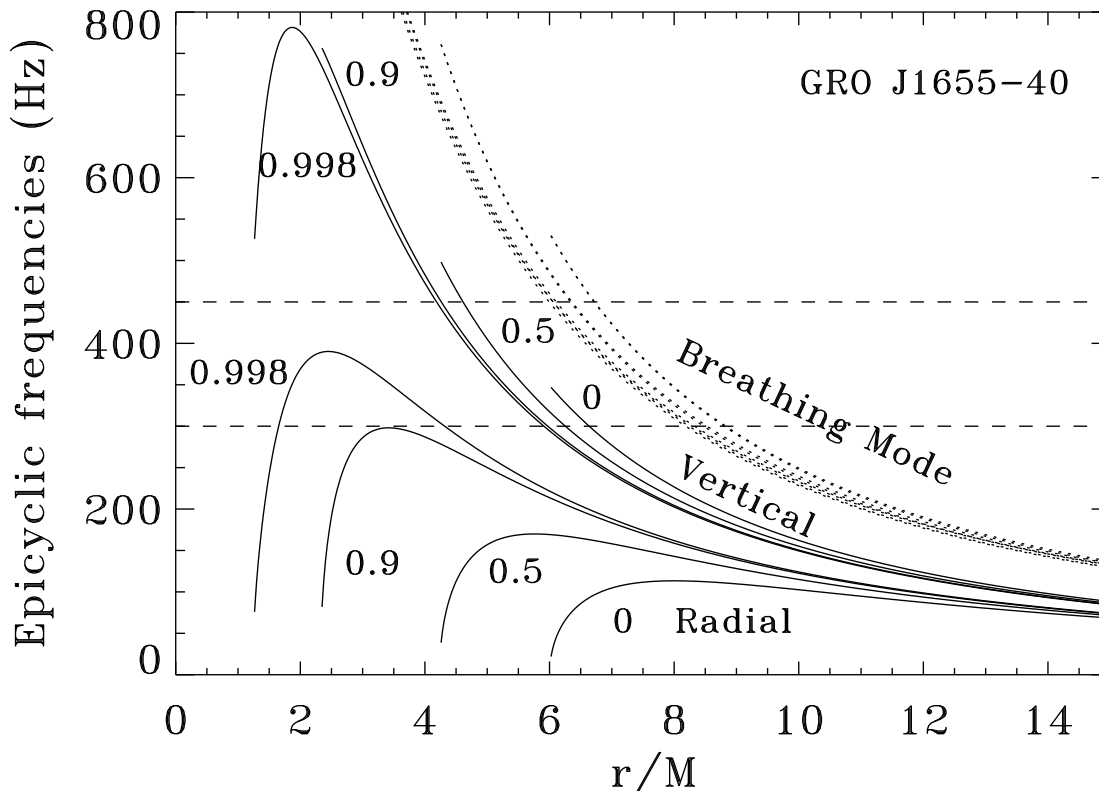


Figure 9. Vertical (upper set of curves) and radial (lower set of curves) epicyclic mode frequencies as a function of Boyer-Lindquist coordinate radius for a black hole of mass $6.3 M_{\odot}$, appropriate for GRO J1655-40, and various black hole spins a/M as labelled. The horizontal dashed lines indicate the frequencies of the observed high frequency QPO's in this source. Models which identify the 300 Hz QPO as the axisymmetric radial epicyclic mode require $a/M \gtrsim 0.9$. Dotted lines show the lowest order breathing mode frequency for the same black hole spins and both constant specific angular momentum tori and tori in the Keplerian limit. Models which identify the 300 Hz QPO with the vertical epicyclic mode and the 450 Hz QPO with the breathing mode can work for any spin.

- Fragile, P. C., 2005, proceedings of the 22nd Texas Meeting on Relativistic Astrophysics, in press [astro-ph/0503305]
 Gammie, C. F., McKinney, J. C., & Tóth, G., ApJ, 589, 444
 Giannios, D., & Spruit, H. C., 2004, A&A, 427, 251
 Goldreich, P., Goodman, J., & Narayan, R., 1986, MNRAS, 221, 339
 Hawley, J. F., & Balbus, S. A., 2002, ApJ, 573, 738
 Ipser, J. R., & Lindblom, L., 1992, ApJ, 389, 392
 Kato, S., 2001, PASJ, 53, 1
 Kato, S., 2005, PASJ, 57, 699
 Kluźniak, W., Abramowicz, M. A., Kato, S., Lee, W. H., & Stergioulas, N., 2004, ApJ, 603, L89
 Kubota, A., & Done, C., 2004, MNRAS, 353, 980
 Lee, W. H., Abramowicz, M. A., & Kluźniak, W., 2004, ApJ, 603, L93
 McClintock, J. E., & Remillard, R. A., 2005, in Lewin W. H. G., van der Klis M., eds., Compact Stellar X-Ray Sources, Cambridge University Press, Cambridge
 Montero, P. J., Rezzolla, L., & Yoshida, S'i., 2004, MNRAS, 354, 1040
 Orosz, J. A., 2003, Proceedings of IAU Symposium 212, eds. K. van der Hucht, A. Herrero, & C. Esteban, San Francisco: Astronomical Society of the Pacific, 365
 Papaloizou, J. C. B., & Pringle, J. E., 1984, MNRAS, 208, 721
 Rezzolla, L., Yoshida, S'i., Maccarone, T. J., & Zanotti, O., 2003a, MNRAS, 344, L37
 Rezzolla, L., Yoshida, S'i., & Zanotti, O., 2003b, MNRAS, 344, 978
 Rubio-Herrera, E., & Lee, W. H., 2005a, MNRAS, 357, L31
 Rubio-Herrera, E., & Lee, W. H., 2005b, MNRAS, submitted
 Schnittman, J. D., & Rezzolla, L., 2005, ApJL, submitted

Seguin, F. H., 1975, *ApJ*, 197, 745

Shafee, R., McClintock, J. E., Narayan, R., Davis, S. W., Li, L.-X., & Remillard, R. A., 2005, *ApJ*, in press

Török, G., 2005, *Astron. Nachr.*, 326, 856

Wagoner, R. V., 1999, *Physics Reports*, 311, 259

Wagoner, R. V., Silbergleit, A. S., & Ortega-Rodríguez, M., 2001, *ApJ*, 559, L25

Zanotti, O., Rezzolla, L., & Font, J. A., 2003, *MNRAS*, 341, 832

Zanotti, O., Font, J. A., Rezzolla, L., & Montero, P. J., 2005, *MNRAS*, 356, 1371